Metal-Free Catalysis

DOI: 10.1002/anie.201103340

Oxygen Insertion Catalysis by sp^2 Carbon**

Benjamin Frank, Raoul Blume, Ali Rinaldi, Annette Trunschke, and Robert Schlögl*

Dedicated to the Fritz Haber Institute, Berlin, on the occasion of its 100th anniversary

Elemental carbon with sp^2 hybridization is omnipresent in our lives, and in its natural form, graphite, an integral part of pencils, batteries, lubricants, steel, and electric motor brushes. High-tech electronic devices and the neutron moderators in nuclear power plants are made of synthetic graphite with a low density of defects (the number of carbon atom dislocations in the hexagonal lattice). Nanostructured sp^2 carbon is used as a pigment (carbon black) and as a polymer filler. The discovery and synthesis of nonplanar carbon allotropes, such as carbon nanotubes (CNTs) and fullerenes,[1] ushered in a new era of cutting-edge applications for elemental carbon. The basic structural unit is graphene,[2] with edge defects and a curvature induced by non-six-membered carbon rings.

In chemistry, graphitic forms of carbon have an intriguing potential for catalysis, with a broad spectrum of application covering hydrogenation, oxidation, polymerization, and chlorination reactions.[3,4] The increased reaction scope has recently been reviewed by Dreyer and Bielawski,[5] who themselves investigated the catalytic activity of graphene oxide in several reactions under mild conditions in the liquid phase.[6] The most prominent example of heterogeneous gas-phase catalysis by carbon materials is the selective oxidative dehydrogenation (ODH) of ethylbenzene to styrene[7,8]—a reaction of high industrial relevance—by nucleophilic oxygen atoms located at the prismatic edges of stacked graphene sheets or at surface defects in the (0001) graphitic surface. For the oxygen-free pathway (DH), the activity of nanocrystalline diamonds coated with defective graphene shells, so-called "bucky diamonds", even exceed the industrial potassium-promoted iron catalyst.[9] It is not surprising that the ODH of light alkanes suffers from a much lower selectivity because the C–H bond in the product molecule is weaker than in the substrate[10]—a common problem in selective oxidation reactions.[11] Point defects filled with electrophilic oxygen likely initiate nonselective combustion pathways. The low-dimensionality of nanostructured carbon materials offers the possibility to modify and optimize the chemical environment of the active sites, and thus to obtain well-defined structure–reactivity correlations. The absence of strongly Lewis-acidic metal cations minimizes the deposition of coke and thus deactivation of the catalyst. This in turn can reduce process costs by not necessitating the addition of steam or periodic regeneration of the catalyst by coke burning.[9] Such progress in ODH and DH catalysis encouraged us to test nanostructured carbon catalysts for oxygen insertion in the selective gas-phase oxidation of acrolein to acrylic acid (AA) as a model reaction [Eq. 1].

$$CH_2{=}CHCHO + {}^1\!/_2\, O_2 \rightarrow CH_2{=}CHCOOH \qquad (1)$$

Here, hydrogen abstraction from the formyl group is followed by oxygenation to form the carboxy group. This industrial process is carried out over optimized Mo/V mixed metal oxide catalysts to provide AA in yields of greater than 95% at temperatures as low as 200–300 °C.[12] The addition of steam to the feed increases the performance and lifetime of the catalysts.[12–14] Graphitic carbon allotropes can resist the oxidative stress under these conditions.[15] However, the use of natural graphite flakes as the heterogeneous catalyst results in a poor C_3H_4O conversion of 0.4% at an AA selectivity of only 37%. A comparison of graphite flakes of different diameter discloses the location of the active sites: decreasing the size of the flakes by using ball-milled synthetic graphite results in an increase in the conversion to 8.8%, while the selectivity is maintained at a moderate level of 66%; this finding indicates that the prismatic edges of stacked graphene layers host the active moieties for this reaction. A pronounced evolution of the catalytic performance is observed, and the initial decay of activity accompanied by an increasing selectivity during the initial 12 h time-on-stream can be related to the (trans)-formation of oxygen species on the carbon surface (see Figure S1 in the Supporting Information) and the healing of point defects. Similar to (bulk) metal oxides, the switch between a reduced and oxidized state during the reaction is realized by reoxidation with gas-phase oxygen. However, in contrast to metal oxides and the related Mars-van Krevelen redox mechanism, the bulk of the graphite catalyst cannot serve as a reservoir for oxygen atoms. Instead, the (0001) graphitic surface, which mediates the dissociative adsorption of oxygen in the combustion of carbon,[16] could take on this role as well as serve as an electron buffer to facilitate the redox process at the active sites. However, the rate of formation of AA of 86.5 μmol $g^{-1}h^{-1}$ on natural graphite is unquestionably poor compared to the industrial and academic state of the art.[12,17]

[*] Dr. B. Frank, Dr. R. Blume, Dr. A. Rinaldi, Dr. A. Trunschke, Prof. Dr. R. Schlögl
Department of Inorganic Chemistry
Fritz Haber Institute of the Max Planck Society
Faradayweg 4-6, 14195 Berlin (Germany)
E-mail: trunschke@fhi-berlin.mpg.de
Homepage: http://www.fhi-berlin.mpg.de/ac/

[**] This work was supported financially by the EnerChem project of the Max Planck Society. We thank D. S. Su and O. V. Khavryuchenko for discussions, and L. I. Csepei for assistance with the experiments. The chemical structures shown in Figures 1, 3, and S3 were created using Jmol open-source software.

Supporting information for this article is available on the WWW under http://dx.doi.org/10.1002/anie.201103340.

The screening of low-dimensional carbon allotropes[18] gives insight into basic structure–activity relationships (Table 1 and see S1 in the Supporting Information). The superior performance is observed for the allotropes with bent

Table 1: Structural data and catalytic performance of various carbon allotropes in the selective oxidation of acrolein to acrylic acid.

Nanocarbon	S_{BET} [$m^2 g^{-1}$]	d[a] [nm]	$X[C_3H_4O]$[b] [%]	S[AA][b] [%]
natural graphite	11.0	123	0.4	37
synthetic graphite	349	6	8.8	66
MWCNT	541	9.9	14	85
fishbone CNF	50	15–20	1.8	35
OLC	315	5–15	4.5	75
nanodiamond	1.7	5–15	3	51
fullerenes	320	0.7	31[c]	41[c]
MCT	5.0	–	5	12
activated carbon	835	–	26[c]	51[c]

[a] Characteristic diameter of the nanostructured carbon as determined by HRTEM, XRD for natural graphite (L_a), and Raman analysis for synthetic graphite (L_a). [b] Determined after 15 h time-on-stream; 5 vol% C_3H_4O/10 vol% O_2/He, 300 °C, 3000 h^{-1}; side products are CO, CO_2, and trace amounts of acetic acid. [c] No stable performance because of severe oxidative degradation (C balance > 100%).

graphene sheets, namely, multiwalled carbon nanotubes (MWCNTs) and onionlike carbon (OLC), whereas the sp^3-hybridized nanodiamonds result in a low selectivity for the formation of AA. Disordered forms of carbon, such as activated carbon, cannot coordinate the selective reaction and, in addition, rapidly deactivate because of oxidative degradation.[15] The rapid loss of activity is also observed with the C_{60} fullerenes, probably with an open-cage structure in the oxidative atmosphere, thus showing that single-shell graphitic allotropes such as fullerenes, graphene, and single-walled CNTs (SWCNTs) cannot resist the oxidative stress at 300 °C and combust within hours. A heterogeneous model catalyst that provides solely the nucleophilic diketonic carbonyl groups[7] (see Figure S3 in the Supporting Information) also shows a low selectivity in the formation of the desired acid. When the number of ketonic and phenolic oxygenated sites, which temperature-programmed desorption (TPD) show decompose to CO at 650–850 °C (see Table S2 in the Supporting Information), are considered, reaction rates of $6.8 \times 10^{-5}\ s^{-1}$ and $1.9 \times 10^{-4}\ s^{-1}$ can be estimated for the reaction with the graphite and the MWCNT catalysts, respectively. The oxygen functionalities located at the edges and defects of the curved graphene layer have a higher intrinsic activity than those terminating the flat (0001) surface. Furthermore, the bent structure induces a remarkable rise in the selectivity for the formation of AA. A pronounced charge location as a consequence of the curvature benefits the adsorption and activation of dioxygen and may control the type of surface species formed to favor the selective turnover. On the planar basal plane, the unselective peroxo species, as the intermediate of O_2 adsorption with stepwise charge transfer [Eq. 2], will be more stable than the epoxy group, which is the product of dissociation, as favored on the curved basal plane because of pronounced charge localization.

$$O_2(g) \rightarrow O_2(s) \rightarrow O_2^-(s) \rightarrow O_2^{2-}(s) \rightarrow O^-(s) \rightarrow O^{2-}(s) \quad (2)$$

The interaction and activation of small molecules such as O_2, H_2O, CO, or CO_2 by the defective (0001) surface has been described theoretically.[19] However, a higher degree of sp^3 hybridization, as present in the active carbon and nanodiamond samples, is detrimental to the selectivity of formation of AA. The moderate performance of fishbone-like carbon nanofibers (CNFs), which solely expose the prismatic edges to the outer tubular surface, further highlights the importance of extended areas of the (0001) basal plane for the reaction. The relatively poor performance of the quinone model catalyst (MCT, macrocyclic trimer) compared to its superiority over other nanocarbon catalysts in the ODH of ethylbenzene[7] is in line with these results and gives rise to the question of whether the presence of nucleophilic quinine groups is also sufficient for the selective oxidation of C_3H_4O to AA. The stability of the catalytic system is confirmed by the long-term reaction over 120 h. High-resolution transmission electron microscopy (HRTEM) and Raman spectroscopy analyses of the catalysts (see Figure S4 in the Supporting Information) show the structural integrity of the most promising MWCNT catalyst as well as the absence of severe surface damage. In accordance with the conditions of the industrial process, we added 5 vol% H_2O to the reaction stream. In the case of the MWCNTs, the conversion of C_3H_4O increased from 14% without addition of H_2O up to 19% in the presence of H_2O. In parallel, the selectivity for AA also increased from 85 to 87%. A further increase in the steam content up to 40% drives the C_3H_4O conversion and AA selectivity up to 24% and 90%, respectively. The improvement of the catalytic performance is related to the modified surface properties of the carbon surface under wet conditions. TPD analysis of the catalysts clearly reveals an increased number of carboxy species on switching from a dry to a wet feed (Figure 1 A,B), whereas the amount of other oxygen surface species remains fairly constant. A similar result is obtained by quasi in situ XPS analysis (Figure 1 C–E), where according to band assignments in the literature,[15] the carboxy band is located at around 533.0–533.5 eV. Accordingly, the C1s range (see Figure S5 in the Supporting Information) is characterized by bands at 286 and 288.5 eV, thus indicating C–O and C=O bonds, respectively, as part of the surface functional groups. Their intensity is higher in the MWCNT catalysts and lower in the graphite catalyst.

This finding conclusively proves the effect of surface acidity, which has been similarly discussed for metal oxide catalysts.[13,20] Water molecules transform Lewis acid sites into Brønsted acids, thus ultimately blocking the centers to total oxidation. The surface protonation further enables the formation of AA from the acrylate surface complex and additional steam favors its desorption by competitive adsorption on the catalyst surface. A shift of the band from 725 to 690 °C, which corresponds to phenol decomposition, is the clearest change in the CO desorption profile (Figure 1 A). The destabilization of these species, which likely represent the

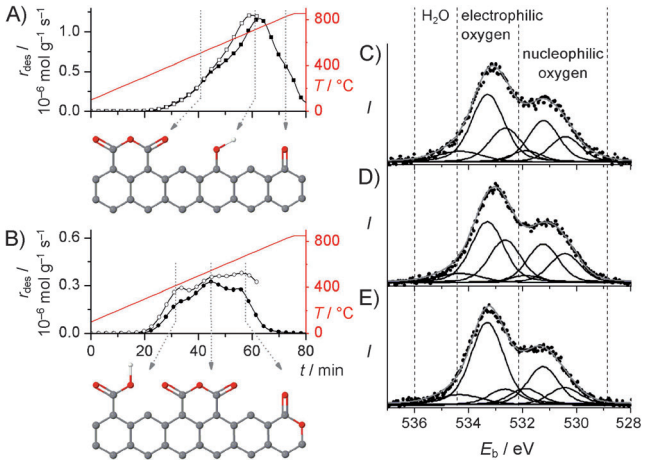

Figure 1. Surface analysis of the catalysts used. A) CO desorption from MWCNTs, indicating the presence of anhydrides (500±120°C), phenols (610±120°C), and ketones/quinones (830±150°C). B) CO_2 desorption from MWCNTs, indicating the presence of carboxylic acids (270±170°C), anhydrides (490±120°C), and lactones (700±110°C).[3] The MWCNTs were pretreated for 15 h at 300°C in a stream of 5 vol% C_3H_4O/10 vol% O_2/He, then cooled in He to 100°C. The TPD profile (filled symbols) was recorded at a heating rate of 10 K min^{-1} (red lines). The experiment was repeated under wet conditions (open symbols), i.e., 5 vol% H_2O was added to the reactant/carrier gas during the pretreatment, cooling, and TPD. The functionalized surface termination is illustrated below the TPD profiles, respectively. C gray, O red, H white. C–E) Synchrotron-excited quasi in situ XP spectra (O1s range) of (C) synthetic graphite and MWCNTs [D) dry, E) wet].

reduced state of the active site, will likely affect their reactivity with oxygen. The positive effect of water on the catalyst reoxidation[15,21] is in line with a number of similarities between metal oxide and carbon-based catalysts.

Steady-state isotopic tracer kinetic analysis (SSITKA; see Figure S6 in the Supporting Information) on switching the $^{16}O_2$ to $^{18}O_2$ reveals the vital exchange of oxygen in the acrolein molecule. This analysis suggests the reversible formation of an acetal-like adsorbate on the carbon surface, whose participation as an intermediate in the selective oxidation remains rather unclear. However, this process results in the formation of singly and doubly labeled AA. Again, this effect is well-known to occur over Mo/V catalysts.[14] Subsequent TPD analysis of the $^{18}O_2$-treated MWCNT catalyst (see Figure S6c,d in the Supporting Information) leads to the identification of O atoms as being responsible for insertion into the substrate. The $^{18}O/^{16}O$ exchange is observed in the low-temperature range of CO and CO_2 desorption, whereas the high-temperature range is dominated by $C^{16}O_x$. This finding suggests that the nucleophilic ketones and quinones, as well as their reduced counterparts phenols, are not removed during the redox cycle of selective C_3H_4O oxidation, in contrast to ODH catalysis which operates at somewhat higher temperature.[22] Indeed, the temperature-programmed reaction of C_3H_4O with the oxygen-treated MWCNTs yields only a small amount of AA (7.3 μmol g^{-1}, see Figure S7 in the Supporting Information), which is in the range of the amount released during the TPD analysis (7.8 μmol g^{-1}). This observation proves that the highly stable ketones (1.4 mmol g^{-1}) will not transfer oxygen to the substrate molecule. Instead, labile electrophilic oxygen atoms likely insert into the formyl C–H bond after its activation by nucleophilic oxygen species. Regarding the fact that high activity/selectivity of carbon allotropes is strictly correlated to the exposition of the (0001) basal plane to the outer surface, we suggest the mobile epoxide C–O–C species, as the electrophilic product of dissociative O_2 adsorption,[16,23] to be responsible for selective turnover. These species are equipped with a high reactivity as a result of severe strain, because the two incorporated carbon atoms change their configuration from a planar sp^2- to a distorted sp^3-hybridized geometry. Indeed, the graphitic epoxide can migrate to the prismatic edges,[16,23] where catalytic transformation takes place, or instead transform to more stable groups (including CO/CO_2 formation) even at temperatures as low as 200°C.[24] The insertion of epoxide oxygen, which is present in graphene oxide, into organic molecules was indicated in a recent report[25] that demonstrates the removal of typical epoxide IR bands on oxidation of benzyl alcohol in the absence of O_2. The removal of such species to leave the intact (0001) basal plane has further been predicted for the reaction of epoxides with adsorbed hydrogen to hydroxyl radicals and/or water.[26]

To localize the active sites at the prismatic edges, we modified the surface of MWCNTs with either 1 wt% B_2O_3 or P_2O_5. It is reported, that these heteroatoms selectively block the zigzag and armchair terminations of graphene sheets, respectively.[27] The decreased C_3H_4O conversions of 6.5% for the B_2O_3/MWCNTs and 5.2% for the P_2O_5/MWCNTs thus provide evidence for the catalytic activity of both configurations. However, the P modification results in an increased AA selectivity (90.9%) compared to the pristine MWCNTs, whereas the B-modified sample shows a lower AA selectivity of 83.9%. This observation suggests that the quinone group located at the zigzag termination of the graphene layer acts more selectively in the C_3H_4O oxidation than the one in the armchair configuration, even though this effect is only weakly pronounced. It should also be considered that this kind of modification also affects the surface acidity and blocks point defects. The robustness of the catalytic system is unique: neither (short-term) harsh oxidative stress nor high-temperature calcination, which substantially defunctionalizes the carbon surface, can induce persistent damage to its catalytic function. The MWCNT catalyst rapidly recovers after treatment in air at 500°C, as well as after TPD in He up to 850°C, and the catalyst approaches its initial activity and selectivity within a few hours (see Figure S8 in the Supporting Information). As compared to metal oxide catalysts, which often comprise several more- or less-active and selective crystallographic phases that may interchange during the course of a reaction and cause irreversible deactivation, the graphitic carbon is the thermodynamically most favorable form of carbon, and thus provides no possibility for structural rearrangement.[10b]

The variation of the gas-hourly space velocity (GHSV) reveals a weakly decreasing AA selectivity as the C_3H_4O conversion increases up to 15% (see Figure S9 in the Supporting Information), which suggests that the formation

of CO_x, the only by-products observed, occurs by direct C_3H_4O combustion, whereas AA is more resistant to total oxidation. In contrast to O_2, the H_2O concentration has a major effect on the product distribution. Thus, the effect of H_2O on the reaction was also investigated by kinetic analysis. The preexponential factor remains fairly constant at around $(3\pm1)\times10^{24}$ molecules $g^{-1}s^{-1}$, which indicates that the number of active sites will not change when switching from the dry to the wet feed. However, the addition of 5% H_2O to the reactant gas mixture significantly lowers the apparent activation energy from 85 to 80 kJ mol^{-1} (Figure 2A). The lowering of the barrier must be attributed to the surface

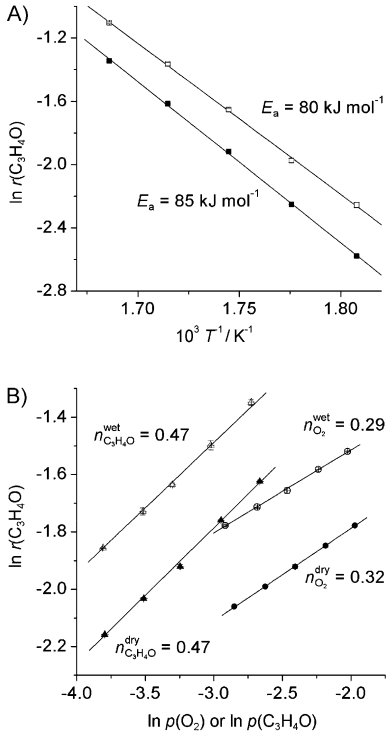

Figure 2. Reaction kinetics of C_3H_4O oxidation. A) Arrhenius plot of the reaction rates under dry (■) and wet (□) conditions at 280–320 °C with a gas feed of 5 vol% C_3H_4O/10 vol% O_2/He. B) Rate of C_3H_4O oxidation as a function of the partial pressure p of O_2 (circles) or C_3H_4O (triangles) over MWCNTs under dry (filled symbols) and wet (open symbols) conditions. The reaction rates were measured at 300 °C. Wet reaction conditions were obtained by adding 5 vol% H_2O to the reaction gas mixture.

acidity induced by surface carboxy groups, which likely affect the adsorption of the reactant and/or the stability of the transition state. The activation energy under dry conditions corresponds to the energy barrier of epoxy group hopping (0.9 eV) as determined by first principles calculations,[23] thus suggesting that oxygen mobility on the (0001) graphitic surface might be the rate-determining factor of the reaction. This is plausible if we consider the reaction to occur at the edge of the basal planes of CNTs. A moderate influence of catalyst reoxidation on the overall rate is confirmed by a kinetic isotope effect (KIE) of $k(^{16}O_2)/k(^{18}O_2)=1.06$ (see Figure S6b in the Supporting Information). The reaction orders for C_3H_4O and O_2 over the MWCNTs under dry conditions are 0.47 and 0.32 (Figure 2B), respectively. Broken rate orders agree with the multistep reaction mechanism and indicate that the carbon surface is almost saturated with C_3H_4O and/or AA. The reaction rate controls the balance between the surface reaction of C_3H_4O with the oxidized carbon surface, the catalyst reoxidation, and the desorption of AA from the active site. The conjugated π electrons of the substrate and reaction product molecules can favor their adsorption on the (0001) basal plane through van der Waals forces. The reaction order of C_3H_4O remains constant in the presence of 5% H_2O, which suggests that C–H activation is not affected. The decrease in the rate order of O_2 to 0.29 can likely be interpreted by the accelerated reoxidation of the carbon surface by the addition of steam, which has also been observed for the combustion of graphitic carbon as well as for the oxidation of VO_x clusters supported on γ-Al_2O_3.[15,21] Taking all these experimental results and theoretic background into account, the pathway shown in Figure 3 for C_3H_4O oxidation is suggested.

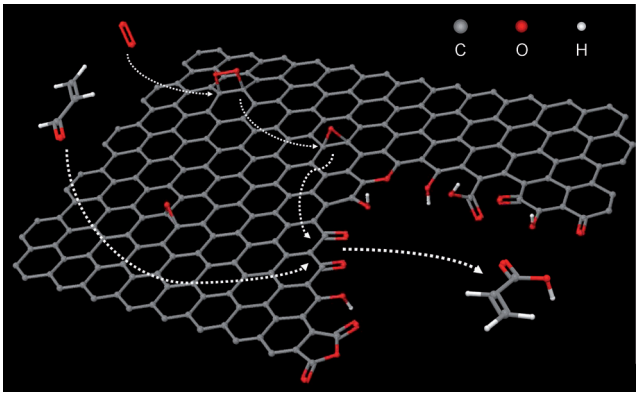

Figure 3. Suggested reaction pathway for the oxidation of C_3H_4O at the graphitic carbon surface. The active domain is illustrated as a rectangular section of a planar graphene sheet with a hole defect, which is terminated by arbitrarily positioned oxygen functionalities. O_2 adsorbs dissociatively at the (0001) surface to form mobile epoxy groups, which migrate to the prismatic edge sites. The adsorption of C_3H_4O at the nucleophilic oxygen sites, i.e., the ketones/quinones, initiates its oxygenation by epoxy oxygen atoms to form acrylic acid.

In conclusion, the element carbon has been demonstrated to be a highly robust and selective catalyst for a model chemical reaction involving the insertion of oxygen into an organic molecule. In the selective oxidation of acrolein, a productivity of 26.5 mmol $g^{-1}h^{-1}$ could be achieved for acrylic acid, which is almost half as high as for the industrial doped MoV mixed oxide (about 60 mmol $g^{-1}h^{-1}$).[12] Fundamental structure–activity relationships enabled the catalytic performance to be optimized with respect to the carbon microstructure and reaction conditions. Such a morphological control on a macroscopic scale is difficult to achieve for metal (oxide) catalysts,[28] thus giving elemental carbon a unique position in catalysis research. In general, carbon catalysis in the absence of polyvalent metal sites with complex electronic and spin structures allows for facile and in-depth theoretical analysis, and thus is an ideal model for understanding reaction mechanisms. In the current study, the reaction mechanism of selective C_3H_4O oxidation could be

clarified. The importance of nucleophilic and electrophilic oxygen species, the prismatic edges as well as the basal planes of graphite, and the abundance of protons being delivered either by carboxy groups or by water were highlighted. Important contributions from ab initio calculations available for the graphene model is an independent basis for interpretation of the experimental data. We could identify substantial similarities between the metal oxide and the carbon-catalyzed reaction, which might help to bridge the gap between these apparently incompatible catalytic systems.

Experimental Section

Catalytic testing: Sample amounts of 500 mg (100–300 μm) were tested in a fixed-bed quartz reactor under atmospheric pressure. The reactor was heated at 5 K min^{-1} up to 300 °C and the feed comprising 5 % C_3H_4O, 10 % O_2, and 0–5 % H_2O in He was dosed by mass-flow controllers (O_2, He) and saturators (H_2O, C_3H_4O) at a total flow of 25 mL min^{-1} (GHSV of 3000 h^{-1}). Kinetic measurements were conducted at 275–325 °C with feed streams of 2–10 % C_3H_4O and 5–20 % O_2 in He. Differential conditions were ensured by an increased total flow of 100 mL min^{-1}, which resulted in C_3H_4O conversions of < 5 %. The reactants and products in the inlet and outlet streams were quantified by an on-line gas chromatograph (Varian CP-4900).

Structural characterization: HRTEM analyses were recorded on a Philips CM 200 LaB6 microscope at an acceleration electron voltage of 200 kV. The specimens were prepared by suspension of the nanocarbon powder in ethanol. Drops of the suspensions were deposited on carbon-enhanced C grids and dried in air. Laser Raman spectroscopy was performed on powder samples by using an ISA LabRam instrument equipped with an Olympus BX40 microscope. The excitation wavelength was 632.8 nm and a resolution of 0.9 cm^{-1} was used. Specific surface areas were determined by N_2 physisorption at −196 °C and calculated from the adsorption branch in the range of $p/p_0 = 0.05$–0.3 by the method of Brunauer, Emmet, and Teller (BET). For XPS and TPD analyses, the samples were cooled down to ambient temperature in the dry and wet feed, respectively. For TPD, the sample was directly subjected to a temperature ramp (10 K min^{-1}) in 25 mL min^{-1} of He. The molecules released from the surface by desorption and/or decomposition of surface species up to 850 °C were quantified by an on-line mass spectrometer and an on-line gas chromatograph, respectively. Synchroton-excited XPS analyses were performed at the ISISS beamline at BESSY II. The compressed sample tablets were analyzed under quasi in situ conditions in an ultrahigh vacuum at 300 °C.

Received: May 16, 2011
Revised: June 9, 2011
Published online: August 16, 2011

Keywords: aldehydes · carbocatalysis · C—H activation · graphite · oxygen

[1] a) S. Iijima, *Nature* **1991**, *354*, 56–58; b) H. W. Kroto, J. R. Heath, S. C. O'Brien, R. F. Curl, R. E. Smalley, *Nature* **1985**, *318*, 162–163.
[2] K. S. Novoselov, A. K. Geim, S. V. Morozov, D. Jiang, Y. Zhang, S. V. Dubonos, I. V. Grigorieva, A. A. Firsov, *Science* **2004**, *306*, 666–669; see also A. K. Geim, *Angew. Chem.* **2011**, *123*, 7100–7122; *Angew. Chem. Int. Ed.* **2011**, *50*, 6966–6985; K. S. Novoselov, *Angew. Chem.* **2011**, *123*, 7123–7141; *Angew. Chem. Int. Ed.* **2011**, *50*, 6986–7002.
[3] P. Serp, J. L. Figueiredo, *Carbon Materials for Catalysis*, John Wiley & Sons, **2009**.
[4] K. P. De Jong, J. W. Geus, *Catal. Rev. Sci. Eng.* **2000**, *42*, 481.
[5] D. R. Dreyer, C. W. Bielawski, *Chem. Sci.* **2011**, *2*, 1233.
[6] a) H.-P. Jia, D. R. Dreyer, C. W. Bielawski, *Tetrahedron* **2011**, *67*, 4431–4434; b) H.-P. Jia, D. R. Dreyer, C. W. Bielawski, *Adv. Synth. Catal.* **2011**, *353*, 528–532; c) D. R. Dreyer, S. Murali, Y. Zhu, R. S. Ruoff, C. W. Bielawski, *J. Mater. Chem.* **2011**, *21*, 3443; d) D. R. Dreyer, S. Park, C. W. Bielawski, R. S. Ruoff, *Chem. Soc. Rev.* **2010**, *39*, 228.
[7] J. Zhang, X. Wang, Q. Su, L. Zhi, A. Thomas, X. Feng, D. S. Su, R. Schlögl, K. Müllen, *J. Am. Chem. Soc.* **2009**, *131*, 11296–11297.
[8] J. Zhang, D. S. Su, A. Zhang, D. Wang, R. Schlögl, C. Hébert, *Angew. Chem.* **2007**, *119*, 7460–7464; *Angew. Chem. Int. Ed.* **2007**, *46*, 7319–7323.
[9] J. Zhang, D. S. Su, R. Blume, R. Schlögl, R. Wang, X. Yang, A. Gajović, *Angew. Chem.* **2010**, *122*, 8822–8826; *Angew. Chem. Int. Ed.* **2010**, *49*, 8640–8644.
[10] a) B. Frank, J. Zhang, R. Blume, R. Schlögl, D. S. Su, *Angew. Chem.* **2009**, *121*, 7046–7051; *Angew. Chem. Int. Ed.* **2009**, *48*, 6913–6917; b) X. Liu, B. Frank, W. Zhang, T. P. Cotter, R. Schlögl, D. S. Su, *Angew. Chem.* **2011**, *123*, 3376–3380; *Angew. Chem. Int. Ed.* **2011**, *50*, 3318–3322; c) B. Frank, M. Morassutto, R. Schomäcker, R. Schlögl, D. S. Su, *ChemCatChem* **2010**, *2*, 644–648.
[11] B. K. Hodnett in *Supported Catalysts and Their Applications* (Eds.: D. C. Sherrington, A. P. Kybett), RSC, **2001**, pp. 1–8.
[12] T. Ohara, T. Sato, N. Shimizu, G. Prescher, H. Schwind, O. Weiberg, K. Marten, H. Greim in *Ullmann's Encyclopedia of Industrial Chemistry*, Wiley-VCH, Weinheim, Germany, **2003**.
[13] J. Tichý, *Appl. Catal. A* **1997**, *157*, 363–385.
[14] P. Kampe, L. Giebeler, D. Samuelis, J. Kunert, A. Drochner, F. Haa, A. H. Adams, J. Ott, S. Endres, G. Schimanke, T. Buhrmester, M. Martin, H. Fuess, H. Vogel, *Phys. Chem. Chem. Phys.* **2007**, *9*, 3577.
[15] B. Frank, A. Rinaldi, R. Blume, R. Schlögl, D. S. Su, *Chem. Mater.* **2010**, *22*, 4462–4470.
[16] R. T. Yang, C. Wong, *Science* **1981**, *214*, 437–438.
[17] M. Sadakane, N. Watanabe, T. Katou, Y. Nodasaka, W. Ueda, *Angew. Chem.* **2007**, *119*, 1515–1518; *Angew. Chem. Int. Ed.* **2007**, *46*, 1493–1496.
[18] O. Shenderova, V. Zhirnov, D. Brenner, *Crit. Rev. Solid State Mater. Sci.* **2002**, *27*, 227–356.
[19] a) M. K. Kostov, E. E. Santiso, A. M. George, K. E. Gubbins, M. B. Nardelli, *Phys. Rev. Lett.* **2005**, *95*, 136105; b) S. M. Lee, Y. H. Lee, Y. G. Hwang, J. R. Hahn, H. Kang, *Phys. Rev. Lett.* **1999**, *82*, 217; c) S. C. Xu, S. Irle, D. G. Musaev, M. C. Lin, *J. Phys. Chem. C* **2009**, *113*, 18772–18777.
[20] T. V. Andrushkevich, *Catal. Rev. - Sci. Eng.* **1993**, *35*, 213–259.
[21] B. Frank, R. Fortrie, C. Hess, R. Schlögl, R. Schomäcker, *Appl. Catal. A* **2009**, *353*, 288–295.
[22] J. Zhang, X. Liu, R. Blume, A. Zhang, R. Schlögl, D. S. Su, *Science* **2008**, *322*, 73–77.
[23] J.-L. Li, K. N. Kudin, M. J. McAllister, R. K. Prud'homme, I. A. Aksay, R. Car, *Phys. Rev. Lett.* **2006**, *96*, 176101.
[24] H.-K. Jeong, Y. P. Lee, M. H. Jin, E. S. Kim, J. J. Bae, Y. H. Lee, *Chem. Phys. Lett.* **2009**, *470*, 255–258.
[25] D. R. Dreyer, H.-P. Jia, C. W. Bielawski, *Angew. Chem.* **2010**, *122*, 6965–6968; *Angew. Chem. Int. Ed.* **2010**, *49*, 6813–6816.
[26] A. Jelea, F. Marinelli, Y. Ferro, A. Allouche, C. Brosset, *Carbon* **2004**, *42*, 3189–3198.
[27] C. Park, R. T. K. Baker, *J. Phys. Chem. B* **1999**, *103*, 2453–2459.
[28] a) X. Xie, Y. Li, Z.-Q. Liu, M. Haruta, W. Shen, *Nature* **2009**, *458*, 746–749; b) A. Celaya Sanfiz, T. W. Hansen, A. Sakthivel, A. Trunschke, R. Schlögl, A. Knoester, H. H. Brongersma, M. H. Looi, S. B. A. Hamid, *J. Catal.* **2008**, *258*, 35–43.

